52nd IEEE Conference on Decision and Control
December 10-13, 2013. Florence, Italy

Model-Based State of Charge Estimation and Observability Analysis of a Composite Electrode Lithium-Ion Battery

Alexander Bartlett[a], James Marcicki[b], Simona Onori[c], Giorgio Rizzoni[a], Xiao Guang Yang[b], Ted Miller[b]

***Abstract*— Composite electrode lithium-ion batteries can offer improved energy and power density, as well as increased cycle life compared to batteries with a single active material electrode. Both available power and cell life are functions of the local current allocated to each composite material, however there are no examples in literature of electrochemical-based models of composite electrode cells that are suitable for estimation and control. We present a reduced order, electrochemical model of a composite $LiMn_2O_4$ - $LiNi_{1/3}Mn_{1/3}Co_{1/3}O_2$ cell that predicts bulk and surface concentrations of each composite material, as well as the local current allocated to each material. Observability properties are analyzed by approximating the system as linear over certain operating conditions. A solution method is developed to use the model in an extended Kalman filter for online state of charge estimation, which is validated with experimental data.**

I. INTRODUCTION

Lithium ion (Li-ion) batteries continue to see increased use in automotive hybrid/electric applications due to their high energy and power densities compared to other chemistries; however accurate state of charge (SOC) estimation is required to utilize the battery power safely and efficiently. Due to their ability to capture the physical electrochemical processes occurring in the battery, increased attention has been given to electrochemical-based models over traditional equivalent circuit models to predict cell performance. For example, it has been shown that with knowledge of the electrode surface concentration, pulse charging that exceeds the manufacture's upper voltage limit can be done without risking lithium plating typically seen with overcharging [1]. Additionally, electrochemical models can be used to improve state of health (SOH) estimation since they utilize physical parameters that evolve as the battery ages, such as the ohmic and charge transfer resistances, amount of cyclable lithium, and volume of active electrode material [9]. Periodic estimates of these parameters can be used to dynamically predict the available capacity and power. Continually updating the model parameters as the battery ages also maintains robust SOC estimation throughout the life of the battery [10]. However, electrochemical models inherently consist of partial differential equations (PDEs) which are not well suited to estimation methods. Therefore, model order reduction techniques can be applied to approximate the governing PDEs while still preserving adequate information for improved SOC/SOH estimates. Electrochemical models also have an advantage over equivalent circuits in that they eliminate the need for complex parameter identification algorithms [21]; although certain electrochemical parameters, such as diffusion coefficients and kinetic rate constants, can be difficult to quantify experimentally [2], [3].

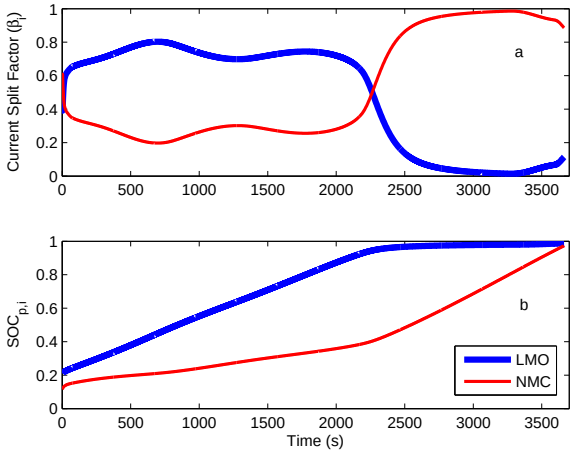

Fig. 1: a) Fraction of the total current through each composite material and b) SOC of each material under a constant 1C discharge, as predicted by the multiple particle, reduced order model.

More sophisticated models are particularly useful in predicting the performance of batteries with composite electrodes. Composite electrodes consist of a blend of two or more electrode chemistries in order to improve performance and life. Layered $LiNi_{1/3}Mn_{1/3}Co_{1/3}O_2$ (NMC), which has a high energy density but poor rate capability [5], has been mixed with $LiMn_2O_4$ spinel (LMO), which has good rate capability but suffers from poor life due to manganese dissolution in the electrolyte [4], [6]. The result is a composite cathode that exhibits good energy and power densities with improved cycle life [7]. However, Li does not necessarily (de)intercalate from each composite material at the same rate. For example, Figure 1 (predicted using the model described in this paper) shows that during a constant current discharge the LMO approaches saturation first, at which point the NMC carries much of the remaining current until the discharge is complete. This same behavior was seen using x-ray diffraction (XRD) to track the structural changes of each cathode material during charge/discharge [5]. Since

This work was supported by the Ford University Research Project

[a] Center for Automotive Research, The Ohio State University, Columbus, OH 43212, USA (bartlett.137, rizzoni.1@osu.edu)

[b] Ford Motor Company, Research and Innovation Center, 2101 Village Rd., Dearborn, MI 48124, USA (jmarcick, xyang11, tmille22@ford.com)

[c] Automotive Engineering Department, Clemson University, Greenville, SC 29607, USA. She was with [a] at the time of this research. sonori@clemson.edu

the instantaneous available power is highly dependent on the remaining capacity of each material, one challenge for estimation of composite material electrodes is to predict the effective SOC of each material, rather than just the SOC of the entire electrode/cell. Additionally, since capacity and power fade of each material are typically functions of the local current throughput, SOH estimation can be improved by modeling how the current is allocated to each material at different SOC and stages of life.

The extended Kalman filter (EKF) has been shown to work well for SOC estimation using equivalent circuit battery models [15]–[17] and single particle electrochemical models (SPM) [1], [12], [19], [21], although it is not necessarily an optimal observer for nonlinear systems. In order to systematically design an observer, the system must be equipped with observability properties. Global observability is almost always straightforward to prove for linear systems [22]; for nonlinear systems, this may not be the case. Local observability of a volume-averaged electrochemical model, similar to the SPM, has been shown in [19]. However, global observability of nonlinear electrochemical-based models is still a topic under investigation.

The novel contributions of this paper include an extension of the reduced order, electrochemical model developed in previous work [8]–[10] to a battery with a composite electrode, in a form suitable for estimation. The model is used to design an EKF to estimate the SOC of each composite material. A method for analyzing observability is presented, and the estimation algorithm is validated with experimental data under dynamic load conditions.

II. METHODS

A. Model Overview

The multiple particle, reduced order, electrochemical model (MPRO) described herein has been used previously by our research group for characterizing aging in cells with composite cathodes [9]. Our goal is to use the MPRO model to design an EKF for online SOC estimation and, in future work, SOH estimation. The model structure, outlined in Figure 2, is based on the *single particle model* [1], [8], [11], [12], [21], which assumes that the 3-dimensional electrode can be lumped into a single, spherical, representative particle. The intercalation current density is assumed to be uniform throughout the thickness of each electrode and zero in the separator. The negative electrode is treated as a single particle, however in order to predict the allocation of current to each composite cathode material, the positive electrode is modeled as two particles acting in parallel, one representing each material. The potential across the two particles is considered constant but the total current is split between each particle according to its effective impedance. An additional extension to the traditional single particle model is the inclusion of simplified liquid phase dynamics in order to improve the model accuracy at high rates ($>$ 1C) [1], [8].

The model governing equations can be found in [9] and will not be repeated here, with the exception of a few clarifications.

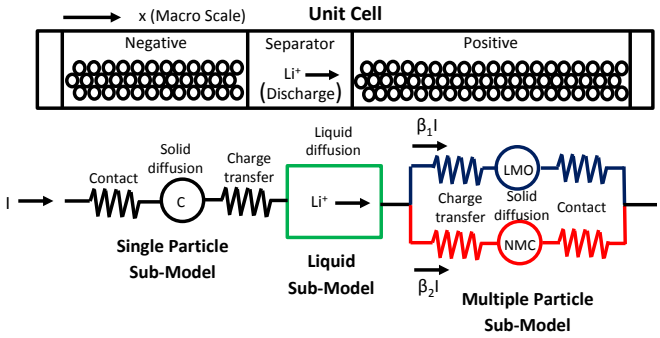

Fig. 2: Schematic of the MPRO model with single/multiple particle approximations of the anode/cathode, respectively, and simplified liquid diffusion dynamics

Ficks law describes the concentration gradient induced diffusion throughout each spherical particle, with the surface concentration flux dictated by the intercalation current density, j_i. Subscript i denotes the negative electrode particle or the two positive electrode particles: n, $p1$, or $p2$, respectively.

$$\frac{\partial c_i}{\partial t} = \frac{D_i}{r}\frac{\partial}{\partial r}\left(r^2\frac{\partial c_i}{\partial r}\right)$$
$$BCs: \ \frac{\partial c_i}{\partial r} = 0 \ at \ r = 0, \ \ D_i\frac{\partial c_i}{\partial r} = \frac{j_i(x,t)}{F} \ at \ r = R_i \tag{1}$$

The intercalation current density, assumed to be piecewise constant throughout each electrode, is scaled by the active electrode volume and surface to volume ratio of the particle:

$$j_i(x,t) = j_i(t) = \frac{I(t)\beta_i R_i}{3AL_i\varepsilon_{am,i}\varepsilon_i} \tag{2}$$

where R_i is the particle radius, A is the current collector area, L_i is the electrode thickness, and $\varepsilon_{am,i}$ is the active material volume fraction. For the positive electrode, a current split factor, β_i, allocates the total current to each particle, and the active material volume incorporates a term for the volume fraction split of each material, ε_i (both β_i and ε_i are equal to 1 for the single negative electrode particle). Since partial differential equations are not well suited for estimation algorithms, the Pade approximation is used to reduce the PDEs to low order ordinary differential equations (ODEs) [13]. The resulting state space formulation is shown for a given particle, subject to a current input, u:

$$\dot{x}_i = A_i x_i + B_i(t)u \tag{3}$$
$$A_i = \begin{bmatrix} 0 & 1 & 0 \\ 0 & 0 & 1 \\ 0 & \frac{1}{b_{3,i}} & \frac{b_{2,i}}{b_{3,i}} \end{bmatrix} \qquad B_i = \begin{bmatrix} 0 \\ 0 \\ \left(\frac{\beta_i(t)R_i}{3FAL_i\varepsilon_{am,i}\varepsilon_i}\right)\frac{1}{b_{3,i}} \end{bmatrix}$$
$$\begin{bmatrix} c_{s,i} \\ \bar{c}_i \end{bmatrix} = \begin{bmatrix} a_{0,i} & a_{1,i} & a_{2,i} \\ a_{0,i} & a_{0,i}b_{2,i} & a_{0,i}b_{3,i} \end{bmatrix} x_i$$
$$\phi_i = U_i(c_{s,i}) - \eta_i(c_{s,i}, \beta_i(t)u) - R_{c,i}\beta_i(t)u \tag{4}$$

The Pade approximation yields the constants a and b, which are functions of the diffusion coefficient and characteristic length (particle radius for spherical diffusion). The linear combination of the states gives either the surface concentra-

tion, $c_{s,i}$, or the bulk concentration, $\bar{c}_i$. The surface or bulk SOC of each particle is then obtained by:

$$SOC_i = \frac{c_{s,i}}{c_{max,i}} \qquad \overline{SOC}_i = \frac{\bar{c}_i}{c_{max,i}} \tag{5}$$

where $c_{max,i}$ is the saturation concentration of the electrode material. Choosing the number of states resulting from each Pade approximation represents a tradeoff between higher accuracy and faster computation. A third order approximation of each spherical diffusion equation is used (resulting in 6 total states for the composite positive electrode), since it shows good accuracy in the frequency range typically seen in an automotive application [8], [13], [14]. The nonlinear output equation governing potential, ϕ_i, is equal to the open circuit voltage (OCV), U_i, minus the charge transfer overpotential, η_i, and an ohmic loss. The output potentials from each sub-model (positive, negative, and liquid) are then summed to obtain the total cell potential:

$$\phi_{cell} = \phi_p - \phi_n - \phi_{liq} \tag{6}$$

B. Solution Method

For the negative electrode and liquid phase sub-models, the state solution can be obtained in discrete time using the forward Euler method; however, for the positive electrode sub-model the current input is multiplied by a time varying current split factor, β_i. Since β_i is unknown, an additional constraint must be imposed that the currents through each particle sum to the total current, i.e. $\beta_1 + \beta_2 = 1$. Due to this constraint, the state solution for the positive electrode can only be obtained through iteration, which is problematic if the model is to be used for dynamic state estimation. Instead, a method is presented that approximates the current split at each time step by linearizing the output equation.

To quickly obtain the state solution for the positive electrode, the assumption is made that the diffusion dynamics are slow compared to changes in charge transfer overpotential, η_i, and current [13]. The output equation (4) can then be linearized at each time step, according to the following procedure:

1) At each time step, k, the surface concentration of each particle is fixed to its value at the previous time step, making $U_{i,k}$ a constant.
2) Since the surface concentration is fixed, $\eta_{i,k}$ is a nonlinear function of current only. It is then linearized for each particle using a Taylor-series expansion about its value at the previous time step, $\eta_{i,k-1}$:

$$\beta_{i,k} I_k \approx g_{i,k} + h_{i,k}(\eta_{i,k} - \eta_{i,k-1}) \tag{7}$$

   where $g_{i,k}$ and $h_{i,k}$ are the resulting constants.
3) The output equation for each particle is now linear, and with the additional constraint that the two current splits sum to 1, the following matrix equation can be solved directly by matrix inversion to obtain the current splits β_1 and β_2:

$$\begin{bmatrix} R_{c,1} + \frac{1}{h_{1,k}} & 0 & 1 \\ 0 & R_{c,2} + \frac{1}{h_{2,k}} & 1 \\ 1 & 1 & 0 \end{bmatrix} \begin{bmatrix} \beta_{1,k} I_k \\ \beta_{2,k} I_k \\ \tilde{\phi}_{p,k} \end{bmatrix} = \begin{bmatrix} U_{1,k} + \frac{g_{1,k}}{h_{1,k}} - \eta_{1,k-1} \\ U_{2,k} + \frac{g_{2,k}}{h_{2,k}} - \eta_{2,k-1} \\ I \end{bmatrix} \tag{8}$$

   Although the linearized positive electrode potential, $\tilde{\phi}_{p,k}$, is also obtained from the matrix inversion, it is discarded at this point; instead, the original nonlinear potential equations are used to predict the output. In other words, the positive electrode sub-model is still treated as a nonlinear system, but with a time varying parameter, β_i, whose value is obtained at each time step through the linearization process. Once β_i is obtained, it is substituted into the state dynamics and the solution can be obtained using the forward Euler method.

C. Observability Analysis

For any observer design, including the EKF, the system must be observable (or at least detectable) to ensure that the state estimate converges to the true state. Local observability of a nonlinear system is typically shown with the use of Lie derivatives to form a gradient operator that must have a rank equal to the number of states [23]. However due to the highly nonlinear nature of the MPRO model output equation, evaluating the Lie derivatives becomes computationally intractable. For this reason, studying the observability of reduced order electrochemical models is still a topic of investigation. We present an approach to prove global observability under certain assumptions for the multiple particle sub-system. Subscript p is dropped in this section for clarity.

The approach relies on the fact that the two nonlinear terms in the output equation, U_i and η_i, can be approximated as linear over operating ranges of SOC and current that are typically seen in a PHEV application (20 - 90% SOC and $\pm$ 10C). The OCV curves for LMO and NMC are roughly linear over certain SOC ranges, as shown in Figure 3. The OCV for LMO can be considered linear from $0.22 < SOC_1 < 0.91$. The OCV for NMC can be split into two linear regions, one from $0.22 < SOC_2 < 0.55$ and one from $0.55 < SOC_2 < 0.91$. After applying linear fits over these regions, the OCVs can be approximated as a linear combination of the states:

$$U_i(x) \approx \frac{m_i a_{0,i}}{c_{max,i}} x_{1,i} + \frac{m_i a_{1,i}}{c_{max,i}} x_{2,i} + \frac{m_i a_{2,i}}{c_{max,i}} x_{3,i} + d_i \tag{9}$$

where m_i and d_i are the slope and y-intercept of the linear OCV fit. The charge transfer overpotential, η_i, is a function of both SOC and current; however over a range of SOC and currents (20 - 90% SOC and $\pm$ 10C), η can be approximated as a purely ohmic resistance, i.e. a linear function of current only. This is shown in Figure 4 for the LMO particle. η_i can

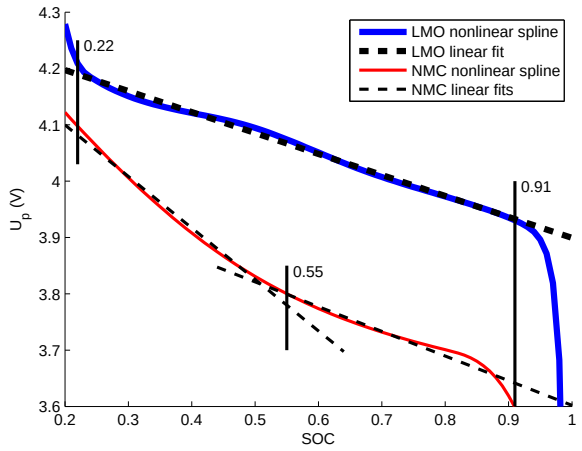

Fig. 3: OCV curves for LMO and NMC, showing regions where the curves are approximately linear. The OCV for NMC must be split into two linear regions.

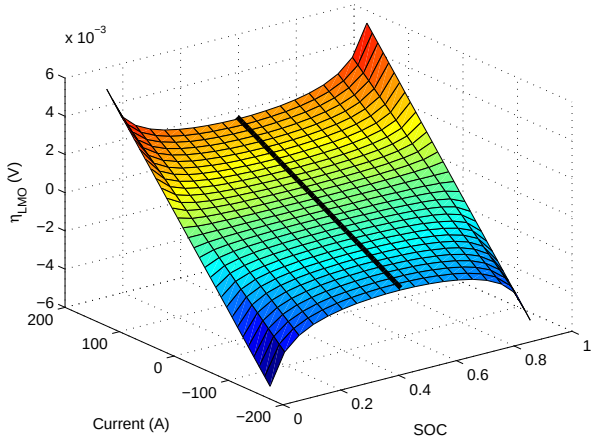

Fig. 4: Variation of η with SOC and current for the LMO particle (NMC shows a similar result). A linear fit is applied at SOC = 0.5 to approximate η as an ohmic resistance over a reasonable range of SOC and current.

then be written as:

$$\eta_i \approx R_{BV,i}\beta_i I \tag{10}$$

where $R_{BV,i}$ is an effective resistance that is calculated by applying a linear fit of η_i and I at a nominal SOC of 0.5. With these approximations, the output equation becomes linear, and it can be written in matrix form:

$$\phi_i \approx \begin{bmatrix} \frac{m_i a_{0,i}}{c_{max,i}} & \frac{m_i a_{1,i}}{c_{max,i}} & \frac{m_i a_{2,i}}{c_{max,i}} \end{bmatrix} x_i + \left[(R_{BV,i}+R_{c,i})\beta_i\right] u + \left[d_i\right]$$
$$= C_i x_i + D_i u + d_i \tag{11}$$

where C_i and D_i are constant matrices. Since the OCV for NMC is split into two linear regions, a C and D matrix can be defined for each SOC range. Now the observability matrix of the linear time invariant system (LTI) can be formed [22]:

$$\theta = \begin{bmatrix} C \\ CA \\ CA^3 \end{bmatrix} \tag{12}$$

The observability matrix has rank 3 for each particle, and SOC range considered, therefore the LTI system is globally observable over these ranges. It should be noted that although the multiple particle sub-model relies on a time-varying current split parameter, β_i, this parameter does not affect the system observability since it only appears in the B and D matrices. Essentially, β_i is considered to be an additional time-varying component of the input u, allowing the system to be treated as LTI. Although this method does not prove observability of the original nonlinear system, some conclusions can be inferred. For example, unlike LMO and NMC, the OCV curve for other cathode materials such as $LiFePO_4$ is very flat [8]. As m_i approaches 0, the observability matrix tends toward losing rank, making observer design more difficult.

D. Estimation Using an Extended Kalman Filter

The Kalman filter is a well-known tool for state estimation of dynamic systems, being the optimal state observer for linear systems with quantifiable process and signal noise that is uncorrelated, white, and Gaussian [15], [17]. Since the output voltage equations are nonlinear, an extended Kalman filter is used, which calculates the feedback gain by approximating the nonlinear system as a linear time varying system. The state dynamics are assumed to exhibit some process noise, that accounts for any disturbances not captured by the model. Likewise, the measurement is assumed to be corrupted with sensor noise. During the prediction step, the model is simulated open loop to obtain a state prediction and output prediction. During the correction step, a correction is applied to the state prediction using proportional feedback from the measured output. The proportional gain is a function of the process and sensor noise covariances, Q and R, respectively. If there is large uncertainty in the model (high Q), the gain will tend to be high, since the state estimate should rely more on the measurement feedback. Conversely, if there is large uncertainty in the measurement (high R), the gain will tend to be low, since more trust should be placed in the open loop model prediction. In practice, Q and R can be difficult to quantify and are typically used as tuning factors to adjust the rate of convergence of the state estimate to the true state.

As shown in the previous section, each particle sub-system can be considered observable with knowledge of the sub-system potential; however the system as a whole is not observable (or can be considered weakly observable [19]) since only the total cell voltage can actually be measured in a real vehicle application. In essence, the measured cell voltage is the sum of each electrode potential and liquid phase potential, so there is no way to uniquely assign the contributions of both electrode and liquid potentials to the overall cell voltage. In light of this, only the positive elec-

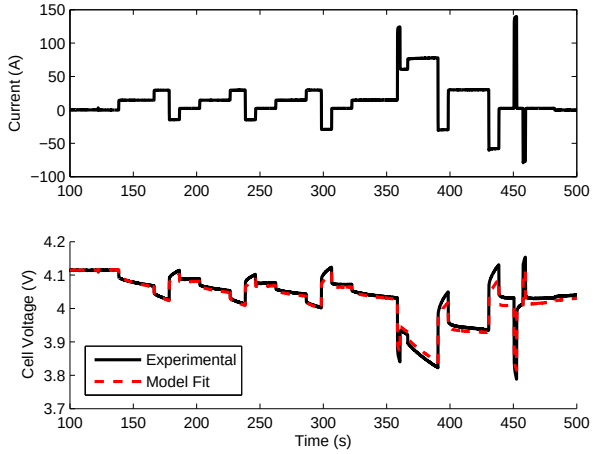

Fig. 5: Model fit to experimental current/voltage data following the USABC, charge depleting PHEV profile. The cycle shown is repeated 7 times until the cell SOC reaches approximately 20%.

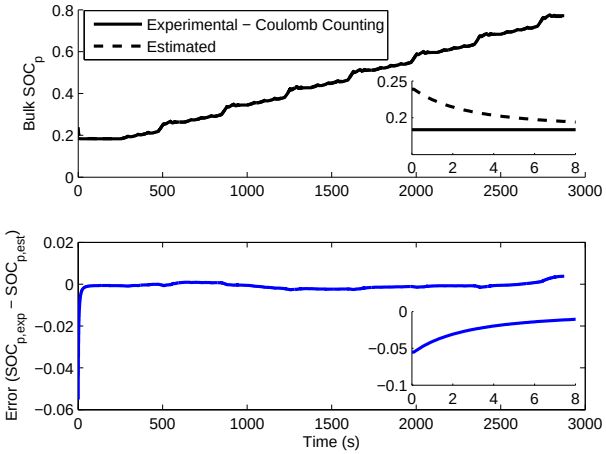

Fig. 6: Bulk SOC_p estimate compared to SOC from Coulomb counting. SOC error is the difference between the estimated SOC and SOC from Coulomb counting. Convergence from incorrect initialization is shown.

trode states are estimated using the EKF. The negative and liquid phase potentials are predicted through an open loop simulation, and are subtracted from the measured cell voltage to obtain a pseudo-measurement of the positive electrode potential, ϕ_p. This is not a true measurement, however, so any model errors in the negative and liquid sub-models will be projected through to adversely affect the positive electrode state estimate. The positive electrode is estimated as it is typically the limiting electrode for instantaneous power, as well as to demonstrate the application of the EKF on the multiple particle sub-system.

E. Experimental Data Collection

A 15 Ah automotive grade pouch cell with composite LMO - NMC cathode and graphite anode is used to generate cell voltage data typical of a PHEV application. The cell is subjected to the charge depleting current profile defined by the United States Advanced Battery Consortium (USABC) [20], as shown in Figure 5, along with the MPRO model prediction. This current profile is repeated 7 times until the cell reaches a SOC of approximately 20%. Parameterization of the model, including half-cell experiments to identify each electrode OCV, is discussed in detail in [9].

III. RESULTS

A. EKF Validation with Experimental Data

The MPRO model outlined above is now used in an EKF to estimate SOC of the positive electrode.

1) EKF Initialization: The sensor noise is quantified by simulating the MPRO model offline with the charge depleting PHEV cycle, and subtracting the cell voltage prediction from the experimental voltage measurement at each time step. The covariance matrix, R, is treated as a constant equal to the covariance of the entire sensor noise vector. In reality, the exact current profile that the vehicle will experience is not available *a priori*, so the exact model voltage prediction error is not known. To account for this, a 10% error is applied to the resulting R matrix. The process noise covariance matrix, Q, is set to zeros since the open loop model predicts SOC very well, assuming perfect state initialization.

It has been shown that, over the life of the battery, Li-consuming side reactions form an inert film at the solid-electrolyte interface (SEI), contributing to capacity loss and causing a shift in the resting SOC of each electrode at a given cell voltage [9]. Therefore, it is important that SOC estimation be robust to initial condition errors. To demonstrate this capability, the state vector is initialized with a 30% error. The state estimate covariance matrix, P_0^+, should be initialized based on the expected initial condition error. Since this is not known *a priori* in a real vehicle application, it is incorrectly initialized to expect a 1% initial state error.

2) EKF Results: Figure 6 shows the resulting bulk SOC_p estimate compared to the SOC obtained by Coulomb counting (integration of the experimentally measured current). The SOC estimate quickly overcomes the initialization error and converges to the true value. The maximum SOC error after convergence is 0.5%. In addition to bulk SOC_p, the model is able to estimate the bulk and surface concentrations of each material, as shown in Figure 7, although these estimates cannot be validated experimentally without the use of XRD or similar techniques. The ability to estimate surface concentrations is useful for powertrain control, since the output voltage, and therefore output power, are functions of the surface concentration of each material.

IV. CONCLUSIONS AND FUTURE WORK

We present a reduced order, electrochemical model extended for composite active materials. A solution method is presented to quickly solve for the current split between the two positive electrode particles. Global observability of the multiple particle sub-system is studied by approximating it as an LTI system over a certain range of operation. The model is then used to design an EKF to estimate both bulk and

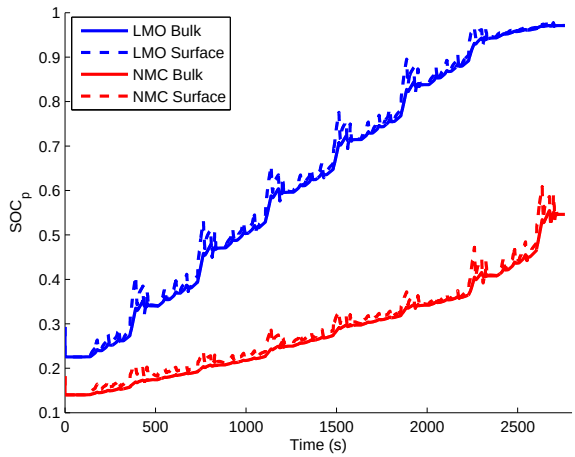

Fig. 7: Bulk SOC and surface SOC estimates for each material.

surface SOC of each material. The bulk positive electrode SOC estimate is validated against experimental data.

Future work in this area will focus on SOH estimation, utilizing the EKF to estimate model parameters that are known to change as the battery ages. Changes in these parameters, such as the total amount of cyclable Li and the active material volume, can be directly related to capacity loss. Furthermore, first-principles based models of degradation mechanisms can add dynamics to the parameter estimation algorithm, improving robustness. System observability will be addressed with the addition of parameter estimation.

V. ACKNOWLEDGMENTS

The authors graciously acknowledge Ford Motor Company for their support via the University Research Project.

REFERENCES

[1] K. Smith, C. Rahn, and C.-Y. Wang, Model-Based Electrochemical Estimation and Constraint Management for Pulse Operation of Lithium Ion Batteries, *IEEE Transactions on Control Systems Tech.*, vol. 18, no. 3, p. 654-663, May 2010.

[2] K. Hatzell, A. Sharma, and H. Fathy, A Survey of Long-Term Health Modeling, Estimation, and Control of Lithium-Ion Batteries: Challenges and Opportunities, *ser. American Control Conference*, Montreal, Canada, June 2012.

[3] M. Smart, J. Whitacre, B. Ratnakumar, and K. Amine, Electrochmeical performance and kinetics of $li_{1+x}(co_{1/3}ni_{1/3}mn_{1/3})1\text{-}xo_2$ cathodes and graphite anodes in low-temperature electrolytes, *J. of Power Sources*, vol. 168, p. 501-508.

[4] Y. Liu, X. Li, H. Guo, Z. Wang. Q. Hu, W. Peng, and Y. Yang, "Electrochemical performance and capacity fading reason of $LiMn_2O_4$/graphite batteries stored at room temperature," *J. of Power Sources*, vol. 189, p. 721-725, 2009.

[5] K.-W. Nam, W.-S. Yoon, H. Shin, K.Y. Chung, S. Choi, and X.-Q. Yang, "*In situ* X-ray diffraction studies of mixed $LiMn_2O_4$-$LiNi_{1/3}Co_{1/3}Mn_{1/3}O_2$ composite cathode in Li-ion cells during charge-discharge cycling," *J. Power Sources*, vol. 192, p. 652-659, 2009.

[6] D. Jang, Y. Shin, and S. Oh, "Dissolution of Spinel Oxides and Capacity Losses in 4 V $Li/Li_xMn_2O_4$ Cells," *J. Electrochem. Soc.*, vol. 143(7), p. 2204-2211, 1996.

[7] S.-H. Park, S.-H. Kang, C.S. Johnson, K. Amine, and M.M. Thackeray, "Lithium-manganese-nickel-oxide electrodes with integrated layered-spinel structures for lithium batteries," *Electrochem. Communications*, vol. 9, p. 262-268, 2007.

[8] J. Marcicki, M. Canova, A.T. Conlisk, G. Rizzoni, "Design and Parametrization Analysis of a Reduced-Order Electrochemical Model of Graphite/$LiFePO_4$ Cells for SOC/SOH Estimation", *J. of Power Sources*, vol. 237, p. 310-324, 2013.

[9] J. Marcicki, A. Bartlett, M. Canova, A.T. Conlisk, G. Rizzoni, Y. Guezennec, X.G. Yang, and T. Miller, Characterization of Cycle-Life Aging in Automotive Lithium-Ion Pouch Cells, *ECS Transactions*, vol. 50(26), p. 235-247, 2013.

[10] J. Marcicki, A. Bartlett, A.T. Conlisk, G. Rizzoni, X.G. Yang, and T. Miller, Robustness Evaluation for State-of-Charge and State-of-Health Estimation Considering Electrochemical Parameter Uncertainties, *presented at the American Control Conference*, Washington, DC, June 2013.

[11] S. Santhanagopalan, Q. Guo, P. Ramadass, and R. White, Review of models for predicting the cycling performance of lithium ion batteries, *J. of Power Sources*, vol. 156, p. 620628, 2006.

[12] S. Santhanagopalan and R. White, "Online estimation of the state of charge of a lithium ion cell," *J. of Power Sources*, vol.161, p. 1346-1355, 2006.

[13] J. Forman, S. Bashash, J. Stein, and H. Fathy, Reduction of an Electrochemistry-Based Li-Ion Battery Model via Quasi-Linearization and Pade Approximation, *J. of the Electrochem. Soc.*, vol. 158(2), p. A93A101, 2011.

[14] S. Onori, P. Spagnol, V. Marano, Y. Guezennec, G. Rizzoni, A new life estimation method for lithium-ion batteries in plug-in hybrid electric vehicles applications, *International J. of Power Electronics*, vol. 4(3), p. 302-319, 2012.

[15] G. Plett, Extended Kalman filtering for battery management systems of LiPB-based HEV battery packs, Part 1. Background, *J. of Power Sources*, vol. 134, p. 252-261, 2004.

[16] G. Plett, Extended Kalman filtering for battery management systems of LiPB-based HEV battery packs, Part 2. Modeling and identification, *J. of Power Sources*, vol. 134, p. 262-276, 2004.

[17] G. Plett, Extended Kalman filtering for battery management systems of LiPB-based HEV battery packs, Part 3. State and parameter estimation, *J. of Power Sources*, vol. 134, p. 277-292, 2004.

[18] S. Rahimian, S. Rayman, and R. White, State of Charge and Loss of Active Material Estimation of a Lithium Ion Cell under Low Earth Orbit Condition Using Kalman Filtering Approaches, *J. of the Electroc. Soc.*, vol. 159(6), p. A860-A872, 2012.

[19] D.D. Domenico, A. Stefanopoulou, and G. Fiengo, Lithium-ion Battery State of Charge and Critical Surface Charge Estimation Using an Electrochemical Model-Based Extended Kalman Filter, *J. of Dynamic Systems, Measurement, and Control*, vol. 132, 2010.

[20] United States Department of Energy Battery Test Manual for Plug-In Hybrid Electric Vehicles, Revision 1, INL EXT-07-12535 (2010).

[21] S.K. Rahimian, S. Rayman, and R. White, Comparison of single particle and equivalent circuit analog models for a lithium-ion cell, *J. of Power Sources*, vol. 196, p. 8450-8462, 2011.

[22] M. Hwang and J.H. Seinfeld, "Observability of Nonlinear Systems," *J. of Optimization Theory and App.*, vol. 10(2), p. 67-77, 1972.

[23] B.L. Walcott, M.J. Corless, and S.H. Zak, "Comparative study of non-linear state-observation techniques," *Int. J. of Control*, vol. 45(6), p. 2109-2132, 1987.